A Theoretical properties

A.1 Derivation of equation (4)

$$E(\hat{r}_{jk}) = 2\big\{\sum_{l=1}^{L}\sum_{m=1}^{L}\Phi_2(-\Delta_{jl}, -\Delta_{km}, \Sigma_{jk}) - \sum_{l=1}^{L}\Phi(-\Delta_{jl})\sum_{m=1}^{L}\Phi(-\Delta_{km})\big\}$$

Proof.

$$\begin{aligned}
E(\hat{r}_{jk}) &= E[(X_{ij} - X_{i'j})(X_{ik} - X_{i'k})] \\
&= 2E(X_{ij}X_{ik}) - 2E(X_{ij})E(X_{ik}) \\
&= 2E\big[\sum_{l=1}^{L} I(Z_{ij} > C_{jl}) \cdot \sum_{m=1}^{L} I(Z_{ik} > C_{km})\big] - 2E\big[\sum_{l=1}^{L} I(Z_{ij} > C_{jl})\big] \cdot E\big[\sum_{m=1}^{L} I(Z_{ik} > C_{km})\big] \\
&= 2\big\{\sum_{1=1}^{L}\sum_{m=1}^{L} P[f_j(Z_{ij}) > \Delta_{jl}, f_k(Z_{ik}) > \Delta_{km}] - \sum_{l=1}^{L} P[f_j(Z_{ij}) > \Delta_{jl}] \cdot P[f_k(Z_{ik}) > \Delta_{km}]\big\} \\
&= 2\big\{\sum_{1=1}^{L}\sum_{m=1}^{L}\Phi_2(-\Delta_{jl}, -\Delta_{km}, \Sigma_{jk}) - \sum_{l=1}^{L}\Phi(-\Delta_{jl})\sum_{m=1}^{L}\Phi(-\Delta_{km})\big\}.
\end{aligned}$$

A.2 Derivation of equation (5)

$$E(\hat{r}_{jk}) = 4\sum_{1=1}^{L}\Phi_2(-\Delta_{jl}, 0, \Sigma_{jk}/\sqrt{2}) - 2\sum_{1=1}^{L}\Phi(-\Delta_{jl}).$$

Proof. Let $U_{ij} = f_j(Z_ij)$ and $V_{ik} = f_k(X_{ik})$. By definition, we have

$$\begin{aligned}
E(\hat{r}_{jk}) &= E[(X_{ij} - X_{i'j})sgn(X_{ik} - X_{i'k})] \\
&= E[X_{ij} \cdot sgn(X_{ik} - X_{i'k})] - E[X_{i'j} \cdot sgn(X_{ik} - X_{i'k})] \\
&= E\big[\sum_{l=1}^{L} I(Z_{ij} > C_{jl}) \cdot sgn(X_{ik} - X_{i'k})\big] - E\big[\sum_{l=1}^{L} I(Z_{i'j} > C_{jl}) \cdot sgn(X_{ik} - X_{i'k})\big] \\
&= \sum_{l=1}^{L}\big\{E[I(Z_{ij} > C_{jl}) \cdot sgn(X_{ik} - X_{i'k})] - E[I(Z_{i'j} > C_{jl}) \cdot sgn(X_{ik} - X_{i'k})]\big\} \\
&= \sum_{l=1}^{L}\big\{E[I(U_{ij} > \Delta_{jl}) \cdot sgn(V_{ik} - V_{i'k})] - E[I(U_{i'j} > \Delta_{jl}) \cdot sgn(V_{ik} - V_{i'k})]\big\}.
\end{aligned}$$

Note that $sgn(x) = 2I(x > 0) - 1$, $(U_{ij}, (V_{ik} - V_{i'k})/\sqrt{2})$ follows standard bivariate Gaussian distribution with correlation $\Sigma_{jk}/\sqrt{2}$ and $(U_{i'j}, (V_{ik} - V_{i'k})/\sqrt{2})$ follows standard bivariate Gaussian distribution with correlation $-\Sigma_{jk}/\sqrt{2}$. Then for each component of summation, we have

$$\begin{aligned}
&E[I(U_{ij} > \Delta_{jl}) \cdot sgn(V_{ik} - V_{i'k})] - E[I(U_{i'j} > \Delta_{jl}) \cdot sgn(V_{ik} - V_{i'k})] \\
=&2E[I(U_{ij} > \Delta_{jl}) \cdot I(V_{ik} - V_{i'k} > 0)] - 2E[I(U_{i'j} > \Delta_{jl}) \cdot I(V_{ik} - V_{i'k} > 0)] \\
=&2\Phi_2(-\Delta_{jl}, 0, \Sigma_{jk}/\sqrt{2}) - 2\Phi_2(-\Delta_{jl}, 0, -\Sigma_{jk}/\sqrt{2}) \\
=&4\Phi_2(-\Delta_{jl}, 0, \Sigma_{jk}/\sqrt{2}) - 2\Phi(\Delta_{jl}).
\end{aligned}$$

Then after the summation of l's, we have equation (5).

A.3 Proof of Lemma II.1 (Monotonically increasing)

$F(t; \boldsymbol{\Delta}_j, \boldsymbol{\Delta}_k) = 2\big\{\sum_{1=1}^{L}\sum_{m=1}^{L} \Phi_2(-\Delta_{jl}, -\Delta_{km}, t) - \sum_{l=1}^{L} \Phi(-\Delta_{jl}) \sum_{m=1}^{L} \Phi(-\Delta_{km})\big\}$ is strictly increasing with respect to t on $(-1, 1)$.

Proof. Notice only the first part $\sum_{1=1}^{L}\sum_{m=1}^{L} \Phi_2(-\Delta_{jl}, -\Delta_{km}, t)$ is related to t. We just need to prove that $\Phi_2(-\Delta_{jl}, -\Delta_{km}, t), \forall k, l$ is strictly increasing, then since the sum of strictly increasing functions is still strictly increasing, we can prove Lemma 2.1.

To show this result, we first note that, for a bivariate random variable (X_j, X_k) with distribution function $\Phi_2(\cdot, \cdot, t)$, the conditional distribution satisfies

$$X_k | X_j = x_j \sim N(tx_j, (1 - t^2)).$$

Note that Δ_{jl}, Δ_{km} are fixed, so the sign of them does not affect the monotonicity of $\Phi_2(\cdot, \cdot, t)$. For notation simplicity, we consider $\Phi_2(\Delta_{jl}, \Delta_{km}, t)$. Then we have,

$$\Phi_2(\Delta_{jl}, \Delta_{km}, t) = \int_{-\infty}^{\Delta_{jl}} \Phi\left(\frac{\Delta_{km} - tx}{\sqrt{1 - t^2}}\right) \phi(x) dx,$$

where $\phi(x)$ is the probability density function of a standard normal variable. Hence,

$$\begin{aligned}
\frac{\partial \Phi_2(\Delta_{jl}, \Delta_{km}, t)}{\partial t} &= \frac{\partial}{\partial t} \int_{-\infty}^{\Delta_{jl}} \Phi\left(\frac{\Delta_{km} - tx}{\sqrt{1 - t^2}}\right) \phi(x) dx \\
&= \int_{-\infty}^{\Delta_{jl}} \frac{\partial}{\partial t}\left[\Phi\left(\frac{\Delta_{km} - tx}{\sqrt{1 - t^2}}\right)\right] \phi(x) dx \\
&= \int_{-\infty}^{\Delta_{jl}} \phi\left(\frac{\Delta_{km} - tx}{\sqrt{1 - t^2}}\right) \phi(x) \frac{-x + t\Delta_{km}}{(1 - t^2)^{2/3}} dx. \qquad (*)
\end{aligned}$$

To discuss the monotonicity of $(*)$, we need to consider two cases.

Case 1. if $\Delta_{jl} < t\Delta_{km}$, then the integration on the right side of $(*)$ is positive. Thus, $\partial \Phi_2 / \partial t > 0$.

Case 2. if $\Delta_{jl} \geq t\Delta_{km}$, then the integration is a decreasing function of Δ_{jl}. This means

$$\begin{aligned}
\partial \Phi_2(\Delta_{jl}, \Delta_{km}, t)/\partial t &\geq \int_{-\infty}^{\infty} \phi\left(\frac{\Delta_{km} - tx}{\sqrt{1 - t^2}}\right) \phi(x) \frac{-x + t\Delta_{km}}{(1 - t^2)^{2/3}} dx \\
&= \frac{\partial}{\partial t} \int_{-\infty}^{\infty} \Phi\left(\frac{\Delta_{km} - tx}{\sqrt{1 - t^2}}\right) \phi(x) dx \\
&= \frac{\partial}{\partial t} \Phi_2(\infty, \Delta_{km}, t) \\
&= 0.
\end{aligned}$$

Therefore, $\Phi_2(\Delta_{jl}, \Delta_{km}, t)$ is strictly increasing with respect to t. Then $F(t, \boldsymbol{\Delta}_j, \boldsymbol{\Delta}_k)$ is strictly increasing.

A.4 Proof of Lemma II.2 (Lipschitz continuous)

Proof. It is sufficient to show that $\exists$ a constant L_2, such that

$$\partial F^{-1}(\tau; \boldsymbol{\Delta}_j, \boldsymbol{\Delta}_k)/\partial \tau < L_2 \Longleftrightarrow \partial F(t; \boldsymbol{\Delta}_j, \boldsymbol{\Delta}_k)/\partial t > 1/L_2, \quad \forall |t| \leq 1 - \delta.$$

Recall, $F(t; \boldsymbol{\Delta}_j, \boldsymbol{\Delta}_k) = 2\big\{\sum\limits_{l=1}^{L}\sum\limits_{m=1}^{L}\Phi_2(-\Delta_{jl}, -\Delta_{km}, t) - \sum\limits_{l=1}^{L}\Phi(-\Delta_{jl})\sum\limits_{m=1}^{L}\Phi(-\Delta_{km})\big\}$. If we can prove for each component $\Phi_2(-\Delta_{jl}, -\Delta_{km}, t), \forall k, l = 1, ..., L$, it satisfies the Lipchitz condition, then F satisfies the Lipschitz condition.

Now, our goal is to show that $\exists \tilde{L} > 0$, for $\forall l, m = 1, ..., L$, such that

$$\partial\Phi_2(-\Delta_{jl}, -\Delta_{km}, t)/\partial t > 1/\tilde{L}, \quad |t| < 1-\delta.$$

Similar to the proof of Lemma 2.2, we need to discuss two cases. Still, the sign of Δ_{jl}, Δ_{km} doesn't matter, we ignore the sign for notation simplicity.

Case 1. $\Delta_{jl} < t\Delta_{km}$, then

$$\partial\Phi_2(\Delta_{jl}, \Delta_{km}, t)/\partial t \geq \int_{-\infty}^{\Delta_{jl}} \phi\left(\frac{\Delta_{km} - tx}{\sqrt{1-t^2}}\right)\phi(x)(-x + t\Delta_{km})dx.$$

Let $\eta = \min\{-|t\Delta_{km}| - 1, \Delta_{jl}\}$. When $x < \eta$, we have $-x + t\Delta_{km} > 1$. Then,

$$\begin{aligned}\frac{\partial\Phi_2(\Delta_{jl}, \Delta_{km}, t)}{\partial t} &\geq \int_{-\infty}^{\eta} \phi\left(\frac{\Delta_{km} - tx}{\sqrt{1-t^2}}\right)\phi(x)dx \\ &\geq \int_{-\infty}^{\eta} \phi\left(\frac{M + |x|}{\sqrt{2\delta - \delta^2}}\right)\phi(x)dx \\ &\geq \int_{-\infty}^{-M-1} \phi\left(\frac{M + |x|}{\sqrt{2\delta - \delta^2}}\right)\phi(x)dx := \frac{1}{L'}.\end{aligned}$$

The second inequality used the property that $\phi(x) = \phi(-x)$ and $\phi(|x|)$ is monotonically increasing. Since $|\Delta_{km}| \leq M$, $|t| \leq 1-\delta$, we have

$$\frac{|\Delta_{km} - tx|}{\sqrt{1-t^2}} \leq \frac{|\Delta_{km}| + |t||x|}{\sqrt{1-t^2}} \leq \frac{M + |X|}{\sqrt{2\delta - \delta^2}}.$$

Case 2. $\Delta_{jl} \geq t\Delta_{km}$, then

$$\begin{aligned}\frac{\partial\Phi_2(\Delta_{jl}, \Delta_{km}, t)}{\partial t} &= \int_{-\infty}^{\Delta_{jl}} \phi\left(\frac{\Delta_{km} - tx}{\sqrt{1-t^2}}\right)\phi(x)\frac{-x + t\Delta_{km}}{(1-t^2)^{2/3}}dx \\ &= \int_{\Delta_{jl}}^{\infty} \phi\left(\frac{\Delta_{km} - tx}{\sqrt{1-t^2}}\right)\phi(x)\frac{-x + t\Delta_{km}}{(1-t^2)^{2/3}}dx \\ \overset{u := x - t\Delta_{km}}{} &= \int_{\Delta_{jl} - t\Delta_{km}}^{\infty} \phi\left(\frac{(1-t^2)\Delta_{km} - tu}{\sqrt{1-t^2}}\right)\phi(u + t\Delta_{km})\frac{u}{(1-t^2)^{2/3}}du \\ \overset{\frac{|(1-t^2)\Delta_{km} - tu|}{\sqrt{1-t^2}} \leq M + \frac{|u|}{\sqrt{2\delta-\delta^2}}}{} &\geq \int_{2M}^{\infty} \phi\left(M + \frac{|u|}{\sqrt{2\delta - \delta^2}}\right)\phi(u + M)udu := \frac{1}{L''}.\end{aligned}$$

Thus, we let $\tilde{L} = max\{L', L''\}$, and $\tilde{L}$ is independent of $\boldsymbol{\Delta}_j, \boldsymbol{\Delta}_k$. Then we have, for $l, m = 1, ..., L$

$$\frac{\partial\Phi_2(\Delta_{jl}, \Delta_{km}, t)}{\partial t} > \frac{1}{\tilde{L}}, \quad |t| \leq 1-\delta.$$

Further, we get

$$\begin{aligned}\frac{\partial F(t; \boldsymbol{\Delta}_j, \boldsymbol{\Delta}_k)}{\partial t} &= \sum_{l=1}^{L}\sum_{m=1}^{L}\frac{\partial}{\partial t}\Phi_2(\Delta_{jl}, \Delta_{km}, t) \\ &\geq L^2 \cdot \frac{1}{\tilde{L}} := \frac{1}{L_2} \qquad L_2 = \tilde{L}/L^2.\end{aligned}$$

A.5 Proof of Theorem II.1 (Convergence)

Lemma A.5.1. *$\Phi^{-1}(y)$ is Lipschitz in $y \in [\Phi(-2M), \Phi(2M)]$, i.e., there exists a Lipschitz constant L_1, such that $|\Phi^{-1}(y_1) - \Phi^{-1}(y_2)| \le L_1|y_1 - y_2|$.*

Proof. It is sufficient to show

$$\frac{d\Phi^{-1}(y)}{dy} \le L_1 \leftrightarrow \phi(x) = \frac{d\Phi(x)}{dx} \ge 1/L_1, \forall x \in [-2M, 2M].$$

It is apparently true if let $L_1 = 1/\phi(2M)$.

Proof of Theorem II.1. Note that $\hat{\Delta}_{jl} = \Phi^{-1}(1 - \frac{1}{n}\sum_{i=1}^n I_{\{X_{ij} \ge l\}})$.

By lemma A.5.1, under the event $A_j := \{|\hat{\mathbf{\Delta}}_j|_\infty \le 2M\}$, we obtain

$$\begin{aligned}
|\hat{\mathbf{\Delta}}_j - \mathbf{\Delta}_j|_\infty &= \max_l |\Phi^{-1}(1 - \frac{1}{n}\sum_{i=1}^n I_{\{X_{ij} \ge l\}}) - \Phi^{-1}(\Phi(\Delta_{jl}))| \\
&\le L_1 \max_l |\frac{1}{n}\sum_{i=1}^n I_{\{X_{ij} \ge l\}} - (1 - \Phi(\Delta_{jl}))|. \quad (**)
\end{aligned}$$

By Hoeffding's inequality, we have

$$\begin{aligned}
P(A_j^c) &= P(|\hat{\mathbf{\Delta}}_j|_\infty \ge 2M) \\
&\le P(|\hat{\mathbf{\Delta}}_j - \mathbf{\Delta}_j|_\infty \ge M) \\
&\le P(\max_l |\frac{1}{n}\sum_{i=1}^n I_{\{X_{ij} \ge l\}} - (1 - \Phi(\Delta_{jl}))| > \frac{M}{L_1}) \\
&\le 2\exp\{-2nM^2/L_1^2\}.
\end{aligned}$$

For any $\epsilon > 0$, the (j,k)th element of $\hat{\Sigma}$ satisfies

$$P(|F^{-1}(\hat{\tau}_{jk}; \hat{\mathbf{\Delta}}_j, \hat{\mathbf{\Delta}}_k) - \Sigma_{jk}| > \epsilon) \le P(\{|F^{-1}(\hat{\tau}_{jk}; \hat{\mathbf{\Delta}}_j, \hat{\mathbf{\Delta}}_k) - \Sigma_{jk}| > t\} \cap A_j \cap A_k) + P(A_j^c) + P(A_k^c).$$

Note $\Sigma_{jk} = F^{-1}(F(\Sigma_{jk}; \hat{\mathbf{\Delta}}_j, \hat{\mathbf{\Delta}}_k); \hat{\mathbf{\Delta}}_j, \hat{\mathbf{\Delta}}_k)$. By Lemma 3.2,

$$\begin{aligned}
&P(\{|F^{-1}(\hat{\tau}_{jk}; \hat{\mathbf{\Delta}}_j, \hat{\mathbf{\Delta}}_k) - \Sigma_{jk}| > \epsilon\} \cap A_j \cap A_k) \\
\le &P(\{L_2|\hat{\tau}_{jk} - F(\Sigma_{jk}; \hat{\mathbf{\Delta}}_j, \hat{\mathbf{\Delta}}_k)| > \epsilon\} \cap A_j \cap A_k) \\
\le &P(L_2|\hat{\tau}_{jk} - F(\Sigma_{jk}; \mathbf{\Delta}_j, \mathbf{\Delta}_k)| > \epsilon/2) \\
+ &P(\{L_2|F(\Sigma_{jk}; \hat{\mathbf{\Delta}}_j, \hat{\mathbf{\Delta}}_k) - F(\Sigma_{jk}; \mathbf{\Delta}_j, \mathbf{\Delta}_k)| > \epsilon/2\} \cap A_j \cap A_k) \\
:= &I_1 + I_2.
\end{aligned}$$

Since $\hat{\tau}_{jk}$ is a U-statistics (unbiased) with bounded kernel, the Hoeffding's inequality for U-statistics yields

$$I_1 \le 2\exp\left(-\frac{n\epsilon^2}{2L_2^2}\right).$$

Let $\Phi_2^1(x,y,t) = \partial\Phi_2(x,y,t)/\partial x$, $\Phi_2^2(x,y,t) = \partial\Phi_2(x,y,t)/\partial y$. For I_2, we have

$$\begin{aligned}
&|F(\Sigma_{jk};\hat{\boldsymbol{\Delta}}_j,\hat{\boldsymbol{\Delta}}_k) - F(\Sigma_{jk};\boldsymbol{\Delta}_j,\boldsymbol{\Delta}_k)|\\
\le& 2\sum_{l=1}^{L}\sum_{m=1}^{L}|\Phi_2(-\hat{\Delta}_{jl},-\hat{\Delta}_{km},\Sigma_{jk}) - \Phi_2(-\Delta_{jl},-\Delta_{km},\Sigma_{jk})|\\
+& 2\sum_{l=1}^{L}\sum_{m=1}^{L}|\Phi(-\hat{\Delta}_{jl})\Phi(-\hat{\Delta}_{km}) - \Phi(-\Delta_{jl})\Phi(-\Delta_{km})|\\
\le& 2\sum_{l=1}^{L}\sum_{m=1}^{L}\{|\Phi_2^1(\xi_{1l})(\hat{\Delta}_{jl}-\Delta_{jl})| + |\Phi_2^2(\xi_{2m})(\hat{\Delta}_{km}-\Delta_{km})|\\
+& |\phi(\xi_{3l})(\hat{\Delta}_{jl}-\Delta_{jl})|\Phi(-\hat{\Delta}_{km}) + \Phi(-\Delta_{jl})|\phi(\xi_{4m})(\hat{\Delta}_{km}-\Delta_{km})|\}\\
\le& 2L^2\{\Phi_2^1(\xi_1)|\hat{\boldsymbol{\Delta}}_j - \boldsymbol{\Delta}_j|_\infty + \Phi_2^1(\xi_2)|\hat{\boldsymbol{\Delta}}_k - \boldsymbol{\Delta}_k|_\infty\\
+& \phi(\xi_3)\max_m \Phi(-\hat{\Delta}_{km})|\hat{\boldsymbol{\Delta}}_j - \boldsymbol{\Delta}_j|_\infty + \phi(\xi_4)\max_l \Phi(-\Delta_{jl})|\hat{\boldsymbol{\Delta}}_k - \boldsymbol{\Delta}_k|_\infty\}.
\end{aligned}$$

Here, the second inequality is because of the Mean Value Theorem.
$\xi_1 = \arg\max_{\xi_{1l}}\Phi_2^1(\xi_{1l})$, $\xi_2 = \arg\max_{\xi_{2m}}\Phi_2^2(\xi_{2m})$, $\xi_3 = \arg\max_{\xi_{3l}}\phi(\xi_{3l})$, $\xi_4 = \arg\max_{\xi_{4m}}\phi(\xi_{4m})$, where ξ_{1l}, ξ_{2m}, ξ_{3l}, ξ_{4m} are the corresponding values from the Mean Value Theorem. Since

$$\Phi_2^1(x,y,t) = \frac{\partial}{\partial t}\int_{-\infty}^{x}\Phi(\frac{y-tz}{\sqrt{1-t^2}})\phi(z)dz = \Phi(\frac{y-tx}{\sqrt{1-t^2}})\phi(x) \le \frac{1}{\sqrt{2\pi}}.$$

Similarly,

$$\Phi_2^2(x,y,t) \le \frac{1}{\sqrt{2\pi}}.$$

Thus, we have

$$|F(\Sigma_{jk};\hat{\boldsymbol{\Delta}}_j,\hat{\boldsymbol{\Delta}}_k) - F(\Sigma_{jk};\boldsymbol{\Delta}_j,\boldsymbol{\Delta}_k)| \le 4L^2\frac{1}{\sqrt{2\pi}}\{|\hat{\boldsymbol{\Delta}}_j - \boldsymbol{\Delta}_j|_\infty + |\hat{\boldsymbol{\Delta}}_k - \boldsymbol{\Delta}_k|_\infty\}.$$

Then,

$$\begin{aligned}
I_2 &\le P(L_2|F(\Sigma_{jk};\hat{\boldsymbol{\Delta}}_j,\hat{\boldsymbol{\Delta}}_k) - F(\Sigma_{jk};\boldsymbol{\Delta}_j,\boldsymbol{\Delta}_k)| > \epsilon/2)\\
&\le P\left(|\hat{\boldsymbol{\Delta}}_j - \boldsymbol{\Delta}_j|_\infty + |\hat{\boldsymbol{\Delta}}_k - \boldsymbol{\Delta}_k|_\infty > \frac{\epsilon\sqrt{2\pi}}{8L^2L_2}\right)\\
&\le P\left(|\hat{\boldsymbol{\Delta}}_j - \boldsymbol{\Delta}_j|_\infty > \frac{\epsilon\sqrt{2\pi}}{16L^2L_2}\right) + P\left(|\hat{\boldsymbol{\Delta}}_k - \boldsymbol{\Delta}_k|_\infty > \frac{\epsilon\sqrt{2\pi}}{16L^2L_2}\right)\\
{}^{by(**)} &\le P\left(L_1\max_l|\frac{1}{n}\sum_{i=1}^{n}I_{\{X_{ij}\ge l\}} - (1-\Phi(\Delta_{jl}))| > \frac{\epsilon\sqrt{2\pi}}{16L^2L_2}\right)\\
&\quad + P\left(L_1\max_l|\frac{1}{n}\sum_{i=1}^{n}I_{\{X_{ik}\ge l\}} - (1-\Phi(\Delta_{km}))| > \frac{\epsilon\sqrt{2\pi}}{16L^2L_2}\right)\\
{}^{Hoeffding} &\le 4\exp\left\{-\frac{n\pi\epsilon^2}{64L^4L_1^2L_2^2}\right\}.
\end{aligned}$$

Therefore,

$$\begin{aligned}
&P(|F^{-1}(\hat{\tau}_{jk};\hat{\boldsymbol{\Delta}}_j,\hat{\boldsymbol{\Delta}}_k) - \Sigma_{jk}| > \epsilon)\\
\le& 2\exp\left\{-\frac{n\epsilon^2}{2L_2^2}\right\} + 4\exp\left\{-\frac{n\pi\epsilon^2}{64L^4L_1^2L_2^2}\right\} + 4\exp\left\{\frac{2nM^2}{L_1^2}\right\},
\end{aligned}$$

which is a uniform bound. Hence, let $\epsilon = c\sqrt{\log(p/n)}$ for some constant c, then $\sup_{j,k} |\hat{R}_{jk} - \Sigma_{jk}| \leq c\sqrt{\log(p/n)}$ with probability greater than $1 - p^{-1}$.

A.6 Proof of Theorem II.2

Let $A_j = \{|\hat{\mathbf{\Delta}}_j|_\infty \leq 2M\}$. From A.4, we have

$$P(A_j^c) \leq 2\exp\{-2nM^2/L_1^2\}.$$

For any $\epsilon > 0$, we can get

$$P(|G^{-1}(\hat{\tau}_{jk}; \hat{\mathbf{\Delta}}_j) - \Sigma_{jk}| > \epsilon) \leq P(\{|G^{-1}(\hat{\tau}_{jk}; \hat{\mathbf{\Delta}}_j) - \Sigma_{jk}| > \epsilon\} \cap A_j) + P(A_j^c).$$

By Lemma II.3,

$$\begin{aligned}
&P(\{|G^{-1}(\hat{\tau}_{jk}; \hat{\mathbf{\Delta}}_j) - \Sigma_{jk}| > \epsilon\} \cap A_j) \\
=&P(\{|G^{-1}(\hat{\tau}_{jk}; \hat{\mathbf{\Delta}}_j) - G^{-1}(G(\Sigma_{jk}; \hat{\mathbf{\Delta}}_j); \hat{\mathbf{\Delta}}_j)| > \epsilon\} \cap A_j) \\
\leq&P(\{L_3|\hat{\tau}_{jk} - G(\Sigma_{jk}; \hat{\mathbf{\Delta}}_j)| > \epsilon\} \cap A_j) \\
\leq&P(L_3|\hat{\tau}_{jk} - G(\Sigma_{jk}; \mathbf{\Delta}_j)| > \epsilon/2) + P(\{L_3|G(\Sigma_{jk}; \hat{\mathbf{\Delta}}_j) - G(\Sigma_{jk}; \mathbf{\Delta}_j)| > \epsilon/2\} \cap A_j) \\
:=&I_1 + I_2
\end{aligned}$$

By Hoeffding's inequality, we can obtain

$$I_1 \leq 2\exp\left\{-\frac{n\epsilon^2}{2L_3^2}\right\}$$

$$\begin{aligned}
&|G(\Sigma_{jk}; \hat{\mathbf{\Delta}}_j) - G(\Sigma_{jk}; \mathbf{\Delta}_j)| \\
\leq&4\sum_{l=1}^{L} |\Phi(-\hat{\Delta}_{jl}, 0, \Sigma_{jk}/\sqrt{2}) - \Phi(-\Delta_{jl}, 0, \Sigma_{jk}/\sqrt{2})| + 2\sum_{l=1}^{L} |\Phi(-\hat{\Delta}_{jl} - \Phi(-\Delta_{jl})| \\
\leq&4\sum_{l=1}^{L} |\Phi_2^1(\xi_{5l})(\hat{\Delta}_{jl} - \Delta_{jl})| + 2\sum_{l=1}^{L} |\phi(\xi_{6l})(\hat{\Delta}_{jl} - \Delta_{jl})| \\
\leq&4L\Phi_2^1(\xi_5)|\hat{\mathbf{\Delta}}_j - \mathbf{\Delta}_j|_\infty + 2L\phi(\xi_6)|\hat{\mathbf{\Delta}}_j - \mathbf{\Delta}_j|_\infty \\
\leq&\frac{6L}{\sqrt{2\pi}}|\hat{\mathbf{\Delta}}_j - \mathbf{\Delta}_j|_\infty.
\end{aligned}$$

Here, the second inequality is still by the mean value theorem, where ξ_{5l}, ξ_{6l} are the corresponding values and $\xi_5 = \arg\max_{\xi_{5l}} \Phi_2^1(\xi_{5l})$, $\xi_6 = \arg\max_{\xi_{6l}} \phi(\xi_{6l})$.

Thus,

$$\begin{aligned}
I_2 &\leq P(L_3|G(\Sigma_{jk}; \hat{\mathbf{\Delta}}_j) - G(\Sigma_{jk}; \mathbf{\Delta_j})| > \epsilon/2) \leq P\left(|\hat{\mathbf{\Delta}}_j - \mathbf{\Delta_j}|_\infty \leq \frac{\epsilon\sqrt{2\pi}}{12LL_3}\right) \\
&\leq 2\exp\left\{-\frac{n\pi\epsilon^2}{36L^2L_1^2L_3^2}\right\}
\end{aligned}$$

Combining I_1, I_2, we have,

$$\begin{aligned}
&P(|G^{-1}(\hat{\tau}_{jk}; \hat{\mathbf{\Delta}}_j) - \Sigma_{jk}| > \epsilon) \\
\leq&2\exp\left\{-\frac{n\epsilon^2}{2L_3^2}\right\} + 2\exp\left\{-\frac{n\pi\epsilon^2}{36L^2L_1^2L_3^2}\right\} + 2\exp\left\{-\frac{2nM^2}{L_1^2}\right\}
\end{aligned}$$

B Simulation studies

In this section, we discussed the effects of the sample size and variable size to the performance of the proposed latent Gaussian copula model. We simulated $n = 100, 200$ and $p = 50, 200, 500$ for the discrete and mixed scenarios in Section 3.1. Figure 1 and 2 compares the ROC curves under various variable sizes for each scenario using every estimators mentioned in Section 3.1, which are:

1. Inverse the Pearson correlation matrix estimator (denote as Pearson estimator) *,
2. Inverse the latent correlation matrix estimator (denote as latent estimator) *,
3. Use the CLIME method (Cai *et al.* 2011) with the Pearson correlation (P-CLIME),
4. Use the CLIME method with the latent correlation (L-CLIME),
5. Use the gLASSO method (Yuan and Lin 2007) with the latent correlation (L-gLASSO),
6. Use the nodewise regression method (Meinshausen and Buhlmann 2006) with the latent correlation (L-NR).

   * The estimator only applies when $n > p$

   ** We also used gLASSO method and nodewise regression method with the Pearson correlation (P-gLASSO, P-NR, respectively) and found the three estimators performed similarly. Hence, we only present the result of P-CLIME for comparison with the latent models.

Table 1 shows the corresponding mean areas under the ROC curve (AUCs). First, we noticed that between the two pairs: Pearson estimator versus Latent estimator and P-CLIME versus L-CLIME, it always has better performance using the latent correlation. As the sample size n increased, the ROC curves improved significantly. When $n = 200$, the AUC scale for the methods using latent correlation is between 0.8 and 0.9, which is statistically good for a classifier. For the low dimension case ($n > p$), the Latent estimator gives the best diagnostic performance, while the L-gLASSO performs poorly for the mixed data case. For the high-dimensional cases, as the variable size p increases, the advantage of using latent correlation has been shown more significantly. The performance of the P-CLIME drops significantly as p increases, while the three latent methods (L-CLIME, L-gLASSO, L-NR) remain steady and similar (L-gLASSO performs better than the other two).

Further, we compared the mean relative errors using Frobenius norm (RF) which is defined as

$$RF = \frac{\|\hat{\Omega} - \Omega\|_F}{\|\Omega\|_F},$$

where $\|A\|_F = \sqrt{\sum_i \sum_j a_{ij}^2}$, $A = (a_{ij})_{p \times p}$. The entries for P-CLIME, L-CLIME, L-gLASSO and L-NR are calculated under the tuning parameter chosen by the HBIC method. The results are given in Table 3, which shows L-gLASSO and L-CLIME have smaller estimation errors than L-NR under all settings. Overall, the L-gLASSO methods have the most steady and accurate performance in high dimensional cases.

C Schizophrenia study

In this section, we provide the whole list of the SNP-ROI interactions in Table 3. Note that the overlapped SNP-ROI interactions are denoted with *.

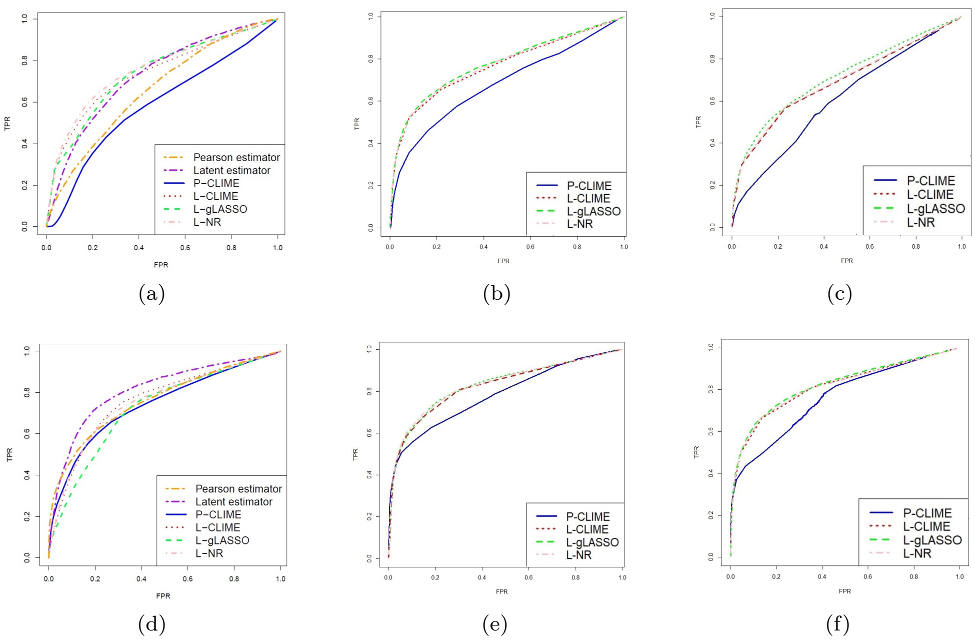

Figure 1: The ROC curves under various settings for $n = 100$. The top row shows the discrete case and the bottom row shows the mixed case. From left to right, $p = 50, 200, 500$, respectively.

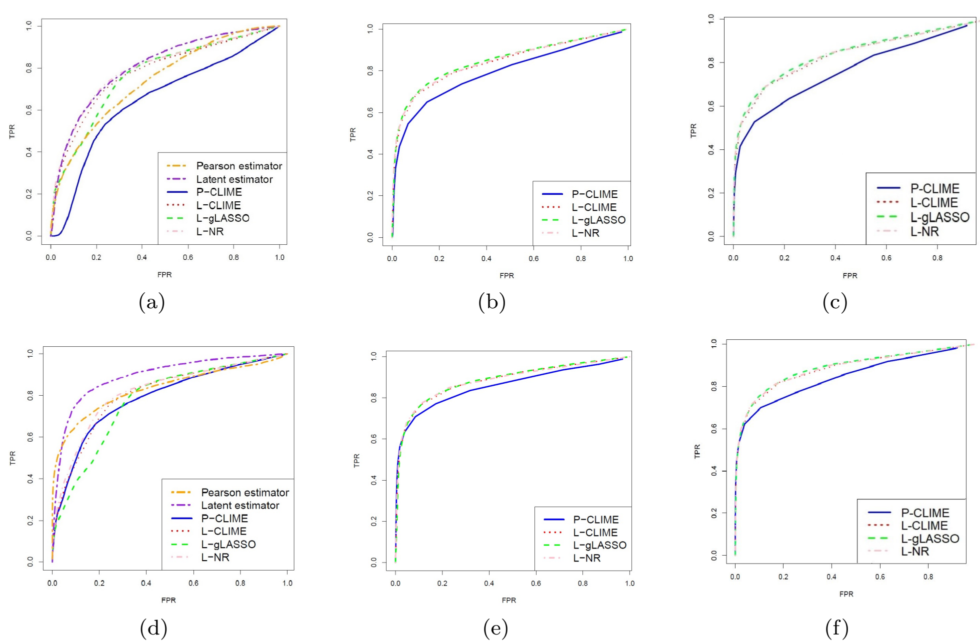

Figure 2: The ROC curves under various settings for $n = 200$. The top row shows the discrete case and the bottom row shows the mixed case. From left to right, $p = 50, 200, 500$, respectively.

Table 1: The mean AUCs of different estimators for various (n, p) settings

		Discrete			Mixed		
n	Method	$p = 50$	$p = 200$	$p = 500$	$p = 50$	$p = 200$	$p = 500$
100	Pearson estimator *	0.676 (0.022)	–	–	0.760 (0.011)	–	–
	Latent estimator *	0.743 (0.027)	–	–	0.816 (0.023)	–	–
	P-CLIME	0.598 (0.046)	0.651 (0.005)	0.476 (0.004)	0.714 (0.016)	0.761 (0.013)	0.622 (0.001)
	L-CLIME	0.746 (0.033)	0.764 (0.011)	0.706 (0.007)	0.758 (0.020)	0.831 (0.009)	0.809 (0.004)
	L-gLASSO	0.745 (0.028)	0.778 (0.010)	0.683 (0.007)	0.717 (0.013)	0.838 (0.009)	0.823 (0.004)
	L-NR	0.765 (0.035)	0.772 (0.013)	0.689 (0.006)	0.754 (0.015)	0.839 (0.008)	0.816 (0.005)
200	Pearson estimator *	0.740 (0.022)	–	–	0.834 (0.019)	–	–
	Latent estimator *	0.807 (0.028)	–	–	0.895 (0.018)	–	–
	P-CLIME	0.640 (0.024)	0.762 (0.014)	0.686 (0.010)	0.779 (0.019)	0.828 (0.009)	0.768 (0.008)
	L-CLIME	0.776 (0.021)	0.837 (0.007)	0.827 (0.005)	0.802 (0.016)	0.876 (0.010)	0.872 (0.004)
	L-gLASSO	0.767 (0.019)	0.852 (0.004)	0.845 (0.004)	0.777 (0.014)	0.885 (0.009)	0.888 (0.005)
	L-NR	0.794 (0.019)	0.848 (0.003)	0.838 (0.005)	0.818 (0.016)	0.884 (0.008)	0.885 (0.004)

* The estimator is only applied when $n > p$, i.e., the setting $(n, p) = (100, 50)$.

Table 2: The average relative estimation errors measured by Frobenius norm (RF)

		Discrete			Mixed		
n	Method	$p = 50$	$p = 200$	$p = 500$	$p = 50$	$p = 200$	$p = 500$
100	Pearson estimator *	2.164 (0.162)	–	–	4.893 (0.492)	–	–
	Latent estimator *	0.813 (0.027)	–	–	0.669 (0.024)	–	–
	P-CLIME	0.632 (0.014)	0.690 (0.001)	2.086 (0.004)	0.566 (0.015)	0.657 (0.005)	2.138 (0.008)
	L-CLIME	0.881 (0.014)	0.924 (0.003)	0.912 (0.002)	0.779 (0.026)	0.870 (0.004)	0.894 (0.003)
	L-gLASSO	0.902 (0.009)	0.927 (0.001)	0.930 (0.003)	0.852 (0.007)	0.873 (0.004)	0.894 (0.004)
	L-NR	1.031 (0.005)	1.014 (0.001)	1.002 (0.001)	1.040 (0.004)	1.027 (0.009)	1.000 (0.001)
200	Pearson estimator *	0.642 (0.007)	–	–	0.580 (0.007)	–	–
	Latent estimator *	0.576 (0.009)	–	–	0.551 (0.005)	–	–
	P-CLIME	0.606 (0.010)	0.663 (0.008)	3.338 (0.035)	0.549 (0.012)	0.579 (0.006)	3.482 (0.019)
	L-CLIME	0.828 (0.019)	0.876 (0.008)	0.893 (0.002)	0.725 (0.023)	0.836 (0.011)	0.865 (0.004)
	L-gLASSO	0.817 (0.022)	0.878 (0.009)	0.895 (0.002)	0.697 (0.024)	0.840 (0.010)	0.868 (0.003)
	L-NR	1.051 (0.016)	1.017 (0.010)	1.002 (0.001)	1.053 (0.015)	1.041 (0.010)	1.037 (0.008)

* The estimator is only applied when $n > p$, i.e., the setting $(n, p) = (100, 50)$.

Table 3: The identified SNP-ROI interactions

	SNP index	Mapped gene	# ROI		MNI		Anatomical location	Network
1	rs6435387	KIF5C	13	-7	-52	61	Precuneus_L	SSN
2	rs7899719	C10orf11	15	0	-15	47	Supp_Motor_Area_L	SSN
3	rs11827962	ANO5 - SLC17A6	15	0	-15	47	Supp_Motor_Area_L	SSN
4	rs16873221	GBA3 - LOC105374524	17	-7	-21	65	Paracentral_Lobule_L	SSN
5	rs3753242	PRKCZ	18	-7	-33	72	Paracentral_Lobule_L	SSN
6	rs1797052	PDZK1	19	13	-33	75	Postcentral_R	SSN
7	rs10924245	KIF26B	21	29	-17	71	Precentral_R	SSN
8	rs13118894	CC2D2A	21	29	-17	71	Precentral_R	SSN
9	rs802568	CNTNAP2	21	29	-17	71	Precentral_R	SSN
10	rs264480	TMEM132D	21	29	-17	71	Precentral_R	SSN
11	rs10924245	KIF26B	22	10	-46	73	Precuneus_R	SSN
12	rs6435387	KIF5C	22	10	-46	73	Precuneus_R	SSN
13*	rs10924245	KIF26B	23	-23	-30	72	Postcentral_L	SSN
14	rs13118894	CC2D2A	23	-23	-30	72	Postcentral_L	SSN
15	rs802568	CNTNAP2	23	-23	-30	72	Postcentral_L	SSN
16	rs264480	TMEM132D	23	-23	-30	72	Postcentral_L	SSN
17	rs17673138	NRG1 - RNU6-663P	24	-40	-19	54	Precentral_L	SSN
18*	rs9599293	LOC105370158, LINC00457	24	-40	-19	54	Precentral_L	SSN
19	rs264480	TMEM132D	37	-38	-15	69	undefined	SSN
20	rs17699030	DOCK6	41	38	-17	45	Precentral_R	SSN
21	rs17255281	SLC19A1, COL18A1	42	-49	-11	35	Postcentral_L	SSN
22	rs264480	TMEM132D	43	36	-9	14	Insula_R	SSN
23	rs286913	EHF	49	19	-8	64	Frontal_Sup_R	CON
24	rs17699030	DOCK6	51	-10	-2	42	Cingulum_Mid_L	CON
25	rs16873221	GBA3 - LOC105374524	53	13	-1	70	Supp_Motor_Area_R	CON
26*	rs17699030	DOCK6	54	7	8	51	Supp_Motor_Area_R	CON
27	rs17699030	DOCK6	55	-45	0	9	Rolandic_Oper_L	CON
28	rs264480	TMEM132D	56	49	8	-1	Insula_R	CON
29	rs17699030	DOCK6	56	49	8	-1	Insula_R	CON
30	rs4611189	LRRC4C	57	-34	3	4	Claustrum_L	CON
31	rs17699030	DOCK6	57	-34	3	4	Claustrum_L	CON
32	rs17699030	DOCK6	60	36	10	1	Insula_R	CON
33*	rs10994397	ANK3	66	-49	-26	5	Temporal_Sup_L	Auditory
34	rs10429924	LOC105373260 - LOC105373262	67	43	-23	20	Rolandic_Oper_R	Auditory
35	rs17069122	MTHFD2P3 - RPL3P7	68	-50	-34	26	SupraMarginal_L	Auditory
36*	rs10924245	KIF26B	70	-55	-9	12	Rolandic_Oper_L	Auditory
37	rs2774292	SYT6 - LOC107985443	73	-30	-27	12	Insula_L	Auditory
38	rs1797052	PDZK1	73	-30	-27	12	Insula_L	Auditory
39	rs1261117	TCF4	73	-30	-27	12	Insula_L	Auditory
40	rs7303433	LOC101928441 - SOX5	74	-41	-75	26	Occipital_Mid_L	Default mode
41	rs7267005	PHF20	74	-41	-75	26	Occipital_Mid_L	Default mode
42	rs17093238	PHF20	74	-41	-75	26	Occipital_Mid_L	Default mode
43	rs2126709	ZNF202	75	6	67	-4	Frontal_Med_Orb_R	Default mode
44	rs264480	TMEM132D	75	6	67	-4	Frontal_Med_Orb_R	Default mode
45	rs7899719	C10orf11	77	-13	-40	1	Precuneus_L	Default mode
46	rs264480	TMEM132D	77	-13	-40	1	Precuneus_L	Default mode
47	rs7246760	LOC100505555 - FBXL12	77	-13	-40	1	Precuneus_L	Default mode
48	rs2774292	SYT6 - LOC107985443	78	-18	63	-9	Frontal_Sup_Orb_L	Default mode
49	rs2774292	SYT6 - LOC107985443	79	-46	-61	21	Temporal_Mid_L	Default mode
50*	rs12325410	LOC101927026	80	43	-72	28	Occipital_Mid_R	Default mode
51	rs264480	TMEM132D	81	-44	12	-34	Temporal_Pole_Mid_L	Default mode
52	rs17699030	DOCK6	81	-44	12	-34	Temporal_Pole_Mid_L	Default mode
53	rs7267005	PHF20	81	-44	12	-34	Temporal_Pole_Mid_L	Default mode
54	rs17093238	PHF20	81	-44	12	-34	Temporal_Pole_Mid_L	Default mode
55	rs2609653	RPL10AP3 - LINC01288	82	46	16	-30	Temporal_Pole_Mid_R	Default mode
56*	rs7303433	LOC101928441 - SOX5	82	46	16	-30	Temporal_Pole_Mid_R	Default mode
57	rs17292804	PPP1R13B	82	46	16	-30	Temporal_Pole_Mid_R	Default mode
58	rs17093238	PHF20	82	46	16	-30	Temporal_Pole_Mid_R	Default mode
59	rs264480	TMEM132D	86	-44	-65	35	Angular_L	Default mode
60	rs11827962	ANO5 - SLC17A6	88	-7	-55	27	Precuneus_L	Default mode
61	rs4611189	LRRC4C	88	-7	-55	27	Precuneus_L	Default mode
62	rs17255281	SLC19A1, COL18A1	88	-7	-55	27	Precuneus_L	Default mode

	SNP index	Mapped gene	# ROI		MNI		Anatomical location	Network
63	rs2774292	SYT6 - LOC107985443	91	-3	-49	13	Precuneus_L	Default mode
64	rs1797052	PDZK1	91	-3	-49	13	Precuneus_L	Default mode
65*	rs2540277	TMEM182	91	-3	-49	13	Precuneus_L	Default mode
66	rs4611189	LRRC4C	91	-3	-49	13	Precuneus_L	Default mode
67	rs4073405	SYT13 - LOC101928812	91	-3	-49	13	Precuneus_L	Default mode
68	rs13118894	CC2D2A	95	11	-54	17	Precuneus_R	Default mode
69	rs10924245	KIF26B	97	23	33	48	Frontal_Sup_R	Default mode
70	rs10924245	KIF26B	98	-10	39	52	Frontal_Sup_Medial_L	Default mode
71	rs1261117	TCF4	98	-10	39	52	Frontal_Sup_Medial_L	Default mode
72	rs10405744	BNIP3P12	101	22	39	39	Frontal_Sup_R	Default mode
73	rs4073405	SYT13 - LOC101928812	103	-10	55	39	Frontal_Sup_L	Default mode
74	rs264480	TMEM132D	109	-3	44	-9	Frontal_Med_Orb_L	Default mode
75*	rs17053965	LOC100129340 - RPSAP49	111	-11	45	8	Cingulum_Ant_L	Default mode
76	rs17255281	SLC19A1, COL18A1	111	-11	45	8	Cingulum_Ant_L	Default mode
77*	rs17053965	LOC100129340 - RPSAP49	112	-2	38	36	Frontal_Sup_Medial_L	Default mode
78	rs17255281	SLC19A1, COL18A1	112	-2	38	36	Frontal_Sup_Medial_L	Default mode
79	rs17255281	SLC19A1, COL18A1	113	-3	42	16	Cingulum_Ant_L	Default mode
80	rs6435387	KIF5C	115	-8	48	23	Frontal_Sup_Medial_L	Default mode
81*	rs11616416	MTUS2	115	-8	48	23	Frontal_Sup_Medial_L	Default mode
82	rs4611189	LRRC4C	118	-58	-30	-4	Temporal_Mid_L	Default mode
83	rs4073405	SYT13 - LOC101928812	120	-68	-41	-5	Temporal_Mid_L	Default mode
84	rs10924245	KIF26B	129	-53	3	-27	Temporal_Mid_L	Default mode
85	rs13118894	CC2D2A	129	-53	3	-27	Temporal_Mid_L	Default mode
86	rs264480	TMEM132D	129	-53	3	-27	Temporal_Mid_L	Default mode
87	rs13118894	CC2D2A	130	47	-50	29	Angular_R	Default mode
88	rs17005123	RNU5A-2P - RASGEF1B	130	47	-50	29	Angular_R	Default mode
89	rs8321	ZNRD1	130	47	-50	29	Angular_R	Default mode
90	rs886424	LINC00243	130	47	-50	29	Angular_R	Default mode
91*	rs17053965	LOC100129340 - RPSAP49	130	47	-50	29	Angular_R	Default mode
92	rs264480	TMEM132D	130	47	-50	29	Angular_R	Default mode
93	rs17005123	RNU5A-2P - RASGEF1B	131	-49	-42	1	Temporal_Mid_L	Default mode
94	rs264480	TMEM132D	133	-2	-35	31	Cingulum_Post_L	Memory retrieval
95	rs17093238	PHF20	136	4	-48	51	Precuneus_R	Memory retrieval
96	rs1797052	PDZK1	144	40	-72	14	Occipital_Mid_R	Visual
97	rs4611189	LRRC4C	146	-8	-81	7	Calcarine_L	Visual
98	rs6576086	TEX22	146	-8	-81	7	Calcarine_L	Visual
99	rs11955175	LOC105374737	147	-28	-79	19	Occipital_Mid_L	Visual
100	rs264480	TMEM132D	147	-28	-79	19	Occipital_Mid_L	Visual
101*	rs7899719	C10orf11	149	-24	-91	19	Occipital_Mid_L	Visual
102	rs1261117	TCF4	149	-24	-91	19	Occipital_Mid_L	Visual
103	rs6435387	KIF5C	155	-14	-91	31	Occipital_Sup_L	Visual
104	rs11038167	TSPAN18	156	15	-87	37	Cuneus_R	Visual
105	rs2774292	SYT6 - LOC107985443	162	24	-87	24	Occipital_Sup_R	Visual
106*	rs12489946	IL20RB - RNA5SP142	163	6	-72	24	Cuneus_R	Visual
107	rs17699030	DOCK6	163	6	-72	24	Cuneus_R	Visual
108	rs2774292	SYT6 - LOC107985443	165	26	-79	-16	Fusiform_R	Visual
109	rs6435387	KIF5C	165	26	-79	-16	Fusiform_R	Visual
110	rs7559992	MPP4	166	-16	-77	34	Cuneus_L	Visual
111	rs10924245	KIF26B	168	-40	-88	-6	Occipital_Mid_L	Visual
112	rs17699030	DOCK6	168	-40	-88	-6	Occipital_Mid_L	Visual
113	rs264480	TMEM132D	171	-26	-90	3	Occipital_Mid_L	Visual
114*	rs6500596	CORO7-PAM16 - DNAJA3	171	-26	-90	3	Occipital_Mid_L	Visual
115	rs6500602	DNAJA3	171	-26	-90	3	Occipital_Mid_L	Visual
116	rs264480	TMEM132D	179	58	-53	-14	Temporal_Inf_R	FPN
117	rs264480	TMEM132D	181	34	54	-13	Frontal_Mid_Orb_R	FPN
118	rs6435387	KIF5C	189	38	43	15	Frontal_Mid_R	FPN
119	rs264480	TMEM132D	190	49	-42	45	Parietal_Inf_R	FPN
120	rs7559992	MPP4	192	44	-53	47	Parietal_Inf_R	FPN
121	rs2126709	ZNF202	192	44	-53	47	Parietal_Inf_R	FPN
122	rs6435387	KIF5C	193	32	14	56	Frontal_Mid_R	FPN
123	rs264480	TMEM132D	194	37	-65	40	Angular_R	FPN
124	rs17255281	SLC19A1, COL18A1	194	37	-65	40	Angular_R	FPN
125	rs13118894	CC2D2A	196	40	18	40	Frontal_Mid_R	FPN
126	rs264480	TMEM132D	196	40	18	40	Frontal_Mid_R	FPN

	SNP index	Mapped gene	# ROI		MNI		Anatomical location	Network
127	rs17053965	LOC100129340 - RPSAP49	199	33	-53	44	Angular_R	FPN
128	rs17255281	SLC19A1, COL18A1	200	43	49	-2	Frontal_Mid_Orb_R	FPN
129	rs4073405	SYT13 - LOC101928812	201	-42	25	30	Frontal_Inf_Tri_L	FPN
130	rs2774292	SYT6 - LOC107985443	202	-3	26	44	Frontal_Sup_Medial_L	FPN
131	rs13118894	CC2D2A	202	-3	26	44	Frontal_Sup_Medial_L	FPN
132	rs17108911	ADRB2 - SH3TC2	202	-3	26	44	Frontal_Sup_Medial_L	FPN
133	rs264480	TMEM132D	202	-3	26	44	Frontal_Sup_Medial_L	FPN
134	rs2774292	SYT6 - LOC107985443	203	11	-39	50	Cingulum_Mid_R	Salience
135	rs16873221	GBA3 - LOC105374524	203	11	-39	50	Cingulum_Mid_R	Salience
136*	rs7899719	C10orf11	203	11	-39	50	Cingulum_Mid_R	Salience
137*	rs4073405	SYT13 - LOC101928812	203	11	-39	50	Cingulum_Mid_R	Salience
138	rs264480	TMEM132D	203	11	-39	50	Cingulum_Mid_R	Salience
139	rs1797052	PDZK1	204	55	-45	37	Parietal_Inf_R	Salience
140	rs13107325	SLC39A8	204	55	-45	37	Parietal_Inf_R	Salience
141	rs1797052	PDZK1	206	31	33	26	Frontal_Mid_R	Salience
142	rs17255281	SLC19A1, COL18A1	209	36	22	3	Insula_R	Salience
143	rs13118894	CC2D2A	210	37	32	-2	Frontal_Inf_Orb_R	Salience
144	rs17108911	ADRB2 - SH3TC2	211	34	16	-8	Insula_R	Salience
145	rs1797052	PDZK1	213	-1	15	44	Supp_Motor_Area_L	Salience
146	rs13118894	CC2D2A	213	-1	15	44	Supp_Motor_Area_L	Salience
147	rs264480	TMEM132D	213	-1	15	44	Supp_Motor_Area_L	Salience
148*	rs13118894	CC2D2A	214	-28	52	21	Frontal_Mid_L	Salience
149	rs16873221	GBA3 - LOC105374524	214	-28	52	21	Frontal_Mid_L	Salience
150	rs264480	TMEM132D	214	-28	52	21	Frontal_Mid_L	Salience
151	rs264480	TMEM132D	215	0	30	27	Cingulum_Ant_L	Salience
152*	rs1797052	PDZK1	217	10	22	27	Cingulum_Ant_R	Salience
153	rs16873221	GBA3 - LOC105374524	217	10	22	27	Cingulum_Ant_R	Salience
154	rs264480	TMEM132D	217	10	22	27	Cingulum_Ant_R	Salience
155	rs1797052	PDZK1	218	31	56	14	Frontal_Mid_R	Salience
156*	rs4073405	SYT13 - LOC101928812	218	31	56	14	Frontal_Mid_R	Salience
157	rs2774292	SYT6 - LOC107985443	219	26	50	27	Frontal_Mid_R	Salience
158	rs7559992	MPP4	222	6	-24	0	Thalamus_R	Subcortical
159	rs13118894	CC2D2A	222	6	-24	0	Thalamus_R	Subcortical
160	rs16873221	GBA3 - LOC105374524	222	6	-24	0	Thalamus_R	Subcortical
161	rs264480	TMEM132D	222	6	-24	0	Thalamus_R	Subcortical
162	rs13332492	CMIP	222	6	-24	0	Thalamus_R	Subcortical
163	rs17255281	SLC19A1, COL18A1	223	-2	-13	12	Thalamus_R	Subcortical
164	rs1797052	PDZK1	226	-5	-28	-4	Midbrain_L	Subcortical
165	rs264480	TMEM132D	226	-5	-28	-4	Midbrain_L	Subcortical
166	rs13118894	CC2D2A	228	-15	4	8	Putamen_L	Subcortical
167	rs17069122	MTHFD2P3 - RPL3P7	230	23	10	1	Putamen_R	Subcortical
168*	rs10924245	KIF26B	236	-56	-50	10	Temporal_Mid_L	Ventral attention
169	rs10924245	KIF26B	237	-55	-40	14	Temporal_Sup_L	Ventral attention
170*	rs10924245	KIF26B	238	52	-33	8	Temporal_Sup_R	Ventral attention
171	rs264480	TMEM132D	256	22	-65	48	Parietal_Sup_R	Dorsal attention
172	rs1797052	PDZK1	258	25	-58	60	Parietal_Sup_R	Dorsal attention
173	rs11827962	ANO5 - SLC17A6	259	-33	-46	47	Parietal_Inf_L	Dorsal attention
174	rs264480	TMEM132D	260	-27	-71	37	Occipital_Mid_L	Dorsal attention
175	rs11827962	ANO5 - SLC17A6	262	-42	-60	-9	Temporal_Inf_L	Dorsal attention
176*	rs4987094	TTC12	243	-16	-65	-20	Cerebellum_6_L	Cerebellar
177	rs11827962	ANO5 - SLC17A6	244	-32	-55	-25	Cerebellum_6_L	Cerebellar
178	rs1797052	PDZK1	245	22	-58	-23	Cerebellum_6_R	Cerebellar
179	rs12282742	SAA2-SAA4, SAA2	245	22	-58	-23	Cerebellum_6_R	Cerebellar
180*	rs2126709	ZNF202	245	22	-58	-23	Cerebellum_6_R	Cerebellar
181	rs802568	CNTNAP2	3	24	32	-18	Frontal_Sup_Orb_R	Uncertain
182	rs264480	TMEM132D	3	24	32	-18	Frontal_Sup_Orb_R	Uncertain
183	rs2245008	LOC105371371	3	24	32	-18	Frontal_Sup_Orb_R	Uncertain
184	rs1792709	LINC01539, LOC102724698	4	-56	-45	-24	Temporal_Inf_L	Uncertain
185	rs11038167	TSPAN18	7	17	-28	-17	ParaHippocampal_R	Uncertain
186	rs12541020	CSMD1	9	65	-24	-19	Temporal_Inf_R	Uncertain
187	rs11038167	TSPAN18	9	65	-24	-19	Temporal_Inf_R	Uncertain
188	rs11827962	ANO5 - SLC17A6	10	52	-34	-27	Temporal_Inf_R	Uncertain
189*	rs11038167	TSPAN18	10	52	-34	-27	Temporal_Inf_R	Uncertain
190	rs17790731	RFESD	12	34	38	-12	Frontal_Inf_Orb_R	Uncertain

	SNP index	Mapped gene	# ROI	MNI			Anatomical location	Network
191	rs264480	TMEM132D	12	34	38	-12	Frontal_Inf_Orb_R	Uncertain
192*	rs6046396	RIN2	84	-58	-26	-15	Temporal_Mid_L	Uncertain
193	rs10924245	KIF26B	85	27	16	-17	Insula_R	Uncertain
194*	rs504918	KALRN	132	-31	19	-19	Frontal_Inf_Orb_L	Uncertain
195	rs1797052	PDZK1	185	35	-67	-34	Cerebellum_Crus1_R	Uncertain
196	rs286913	EHF	185	35	-67	-34	Cerebellum_Crus1_R	Uncertain
197	rs2774292	SYT6 - LOC107985443	250	-50	-7	-39	Temporal_Inf_L	Uncertain
198*	rs1797052	PDZK1	253	-47	-51	-21	Temporal_Inf_L	Uncertain
199	rs286913	EHF	253	-47	-51	-21	Temporal_Inf_L	Uncertain
200	rs6576086	TEX22	254	46	-47	-17	Temporal_Inf_R	Uncertain

* denotes the overlapped SNP-ROI pair from L-gLASSO and P-gLASSO.

References

Cai, T., Liu, W., and Luo, X. (2011). Aconstrained l1 minimization approach to sparse precision matrix estimation. *J. Am. Statist. Ass.*, **106**, 594–607.

Meinshausen, N. and Buhlmann, P. (2006). High-dimensional graphs and variable selection with the lasso. *Annals of Statistics*, **34**, 1436–1462.

Yuan, M. and Lin, Y. (2007). Model selection and estimation in the gaussian graphical model. *Biometrika*, **94**, 19–35.